An Inter-Laboratory Study of Zn−Sn−Ti−O Thin Films using High-Throughput Experimental Methods

Jason R. Hattrick-Simpers,[†] Andriy Zakutayev,[‡] Sara C. Barron,[†] Zachary T. Trautt,[†] Nam Nguyen,[†] Kamal Choudhary,[†] Brian DeCost,[†] Caleb Phillips,[‡] A. Gilad Kusne,[†] Feng Yi,[†] Apurva Mehta,[§] Ichiro Takeuchi,[∥] John D. Perkins,[‡] and Martin L. Green*,[†]

[†]National Institute of Standards and Technology (NIST), Gaithersburg, Maryland 20899-3460, United States
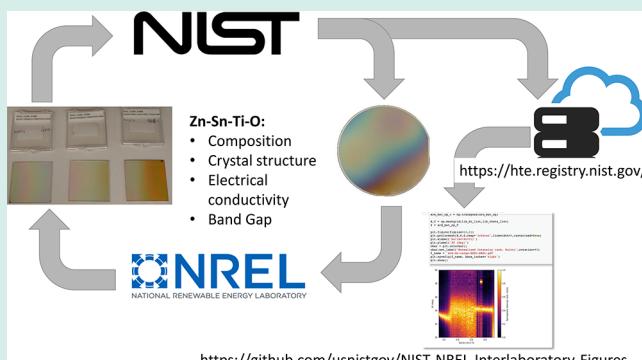[‡]National Renewable Energy Laboratory (NREL), Golden, Colorado 80401, United States
[§]SLAC National Accelerator Laboratory, Menlo Park, California 94025, United States
[∥]University of Maryland, College Park, Maryland 20742, United States

S *Supporting Information*

ABSTRACT: High-throughput experimental (HTE) techniques are an increasingly important way to accelerate the rate of materials research and development for many technological applications. However, there are very few publications on the reproducibility of the HTE results obtained across different laboratories for the same materials system, and on the associated sample and data exchange standards. Here, we report a comparative study of Zn−Sn−Ti−O thin films materials using high-throughput experimental methods at National Institute of Standards and Technology (NIST) and National Renewable Energy Laboratory (NREL). The thin film sample libraries were synthesized by combinatorial physical vapor deposition (cosputtering and pulsed laser deposition) and characterized by spatially resolved techniques for composition, structure, thickness, optical, and electrical properties. The results of this study indicate that all these measurement techniques performed at two different laboratories show excellent qualitative agreement. The quantitative similarities and differences vary by measurement type, with 95% confidence interval of 0.1−0.2 eV for the band gap, 24−29 nm for film thickness, and 0.08 to 0.37 orders of magnitude for sheet resistance. Overall, this work serves as a case study for the feasibility of a High-Throughput Experimental Materials Collaboratory (HTE-MC) by demonstrating the exchange of high-throughput sample libraries, workflows, and data.

KEYWORDS: interlaboratory, high throughput, thin-film sample libraries, data exchange, collaboration

INTRODUCTION

High-throughput experimental (HTE) techniques are an increasingly important way to accelerate the rate of materials research and development for many possible applications.[1,2] In the case of thin film research, HTE methods include combinatorial depositions of sample libraries with composition spreads, spatially resolved characterization for their chemical composition, crystal structure, and relevant properties, as well as corresponding analysis of the high-volume data. Multiple review papers have been published summarizing these thin film HTE methods and their use in different applications across different materials systems.[3−6] However, there are very few publications on the reproducibility of the HTE results obtained across different laboratories for the same materials system used in the same application.[7−10] The corresponding exchange protocols for sample and data have not been reported either. Such a study, reported here, is aimed at increasing the confidence of the broader research community in HTE methods as applied to thin film materials science, and at testing possible data and sample exchange protocols.

In addition to interlaboratory comparison of measurement methods, this study also serves as a proof of concept for a distributed network of high-throughput experimental synthesis and characterization instruments named "High-Throughput Experimental Materials Collaboratory" (HTE-MC).[4] For example, HTE-MC would permit an industrial participant to request HTE libraries of specific materials to be deposited by a HTE-MC member with expertise in combinatorial reactive sputtering. The sample libraries could then be transferred to a synchrotron national user facility for detailed structural studies, then to a national lab with expertise in property measurements, and finally to an academic partner for material degradation studies. For the HTE-MC to function smoothly, standards for

exchanging HTE libraries, data, and measurement protocols will need to be implemented at all partner laboratories. Each measurement would have to be made at identical positions on the same library, ensuring that different measurements can be compared to each other. But even in this case, differences in measured values for the same property can be expected, as different laboratories may employ different characterization methods. This Research Article represents an example of sample exchange, data exchange, and quantitative comparison of results between two laboratories, which enabled the testing of geographically distributed high-throughput experimental measurements.

For the interlaboratory comparative experiments reported in this Research Article, we chose Zn−Sn−Ti−O materials, because it is a pseudoternary oxide system composed of common metallic elements that can be codeposited using different thin film synthesis techniques. Other chemistries (e.g., open-shell transition metal oxides[8,11] or main group sulfides[12,13]) may pose more cross-contamination constraints on available deposition techniques. The other reason for choosing the Zn−Sn−Ti−O material system is that it is chemically similar to several other transparent conductive oxides (TCO)[14] and amorphous oxide semiconductors (AOS).[15] From the practical point of view, TCO are an important class of materials for contact applications in optoelectronic devices (photovoltaics, light-emitting diodes), and AOS are used for transparent transistors in display applications (liquid crystal displays, touch-screens). The corresponding relevant materials properties are optical transparency and electrical conductivity, in addition to crystal structure and chemical composition. However, in contrast to many other main-group pseudoternary oxides,[16,17] there are no previous published reports on Zn−Sn−Ti−O studied using high-throughput combinatorial experimental techniques.

In this interlaboratory study, National Institute of Standards and Technology (NIST) and National Renewable Energy Laboratory (NREL) each synthesized Zn−Sn−Ti−O films with the deposition tools available. Each laboratory then characterized the sample libraries for their composition, structure, thickness, and optical properties on their own previously defined sampling grid. The sample libraries were exchanged, along with the appropriate map coordinates, and the other laboratory performed measurements at the same points as the first laboratory. For some of the measurements, the laboratories used a different measurement system (e.g., spectroscopic ellipsometry versus transmission-reflection optical spectroscopy) with its own unique measurement geometry and analysis protocols. It was found that qualitative compositional trends of the measured properties were well replicated between the two laboratories. Quantitative comparisons of the physical properties varied depending on the measured property and confirmed well-known systematic errors of techniques. Several additional lessons were learned during the study and are discussed in this Research Article.

■ METHODS

At NIST a single Zn−Sn−Ti−O thin film sample library was deposited as a layered continuous composition spread via pulsed laser deposition from 2.54 cm diameter ZnO, SnO$_2$, and TiO$_2$ targets onto a 7.62 cm diameter c-cut (0001) sapphire (Al$_2$O$_3$) wafer. All targets were purchased from commercial vendors with nominal purities greater than 99.9%. The film was deposited in 10^{-3} Torr of O$_2$ at a substrate temperature of 500

°C. The deposition method was described in a previous publication.[18] Briefly, the three targets were located on a rotating carousel and ablated sequentially using a single KrF pulsed laser source with wavelength of ∼248 nm. A pulse laser energy of 200 mJ and a 10 Hz repetition rate were used. The number of pulses for each target was calibrated to provide a 0.5 nm maximum thickness per target per layer. Composition spreads are created by using noncentered deposition in conjunction with substrate rotations coordinated with the target changes. The resulting library exhibited a lateral composition spread that spanned a maximum composition range of 30 cation at.% for Ti, 80 cation at.% for Zn, and 90 cation at.% for Sn with a maximum total film thickness of 140 nm. For these libraries, the composition spread is formed from the inherent nonlinear spatial variation of the deposition process. Accordingly, the change in cation concentration change per millimeter is location-dependent and hence not explicitly reported. Postdeposition, the sample library was cooled under vacuum with no postannealing performed. The NIST library was characterized using a suite of spatially resolved measurement tools at 177 individual locations (spots).

All characterization performed at NIST was performed as follows. The crystal structure of each spot was characterized with spatially resolved X-ray diffraction (Cu K-alpha line) using a Bruker D8 Discover. Chemical composition was determined using wavelength dispersive spectroscopy (WDS) on a JEOL 8900 R electron probe microanalyzer calibrated with elemental Zn, Sn, and Ti standards. The film thickness and optical constants were measured by scanning ellipsometry (J. A. Woollam Co. M-2000 X). Sheet resistance mapping was performed with a Four Dimensions 280DI 4-point probe sheet resistance mapping system with a probe radius of 100 μm and probe spacing of 1 mm. Prior to sheet resistance mapping of each sample library, the measurement system was calibrated with Si reference sample (Model RS 3-0.01, Serial 8155-019). The thickness of the film at each measurement point was used to calculate the conductivity.

NIST clustering of the X-ray diffraction data was performed on background subtracted patterns using the hierarchical clustering function in the Combiview program[19] on the integrated 1-D X-ray diffraction patterns using the Spearman distance metric and average linkages between clusters. Film thickness and absorption coefficient spectra were extracted from position-dependent spectroscopic ellipsometry measurements taken on the library using the CompleteEASE software package; details of this fitting can be found in the Supporting Information. The visible portion of the spectra was first fit by treating the film and substrate as transparent layers. The substrate was fit with the Cauchy dispersion equation and the film−substrate bilayer film was fit as a combined Cauchy−Tauc Lorentz model. To enable an automated determination of the band gap that can be applied equally well to the NIST and NREL measured spectra, the band gaps reported in subsequent sections were taken to be the photon energy at which the optical absorption coefficient equaled about 10^4 cm^{-1}.

At NREL three Zn−Sn−Ti−O thin film sample libraries were deposited by radiofrequency (RF) sputtering from 50 mm diameter ZnO, SnO$_2$, and TiO$_2$ targets on to 50 × 50 mm Eagle XG glass substrates heated to 300 °C in a 10^{-3} Torr of Ar atmosphere. The ZnO and SnO$_2$ targets, held at 16 to 50 W power, were positioned at 30° with respect to the substrate

plane, resulting in 30 cation at. % to 50 cation at.% composition spread across the 50 mm library. The TiO_2 target, held at 33 W power was at 60° with respect to the substrate plane, resulting in nearly constant 5 cation at.% composition across each library. The 60 min duration of the deposition resulted in 200−400 nm thin films. More details about this combinatorial thin film deposition chamber at NREL have been previously reported.[20,21]

All thin films libraries were characterized at NREL as a function of position for crystal structure using spatially resolved X-ray Diffraction (XRD − Bruker D8 Discover), for chemical composition and thickness using X-ray Fluorescence Spectroscopy (XRF−Fischerscope XDV-SDD), for optical transmittance and reflectance using UV−vis spectroscopy (custom, with Ocean Optics spectrometers), for sheet resistance using four-point probe instrument (custom, with Signatone probe head). The thickness was determined from XRF measurements and material density by the software on the instrument, using the previously published model.[22] All measurements were processed into the NREL High-Through-put Experimental Materials Database (HTEM-DB) with automatic normalization for measurement time and sample thickness as well as background subtraction for a glass substrate.[21] Data was obtained from the HTEM-DB API for analysis. The thickness obtained from the XRF measurements was used to calculate the conductivity from the measured sheet resistance and the absorption coefficient from the measured reflection and transmission spectra. More information about these spatially resolved characterization instruments at NREL can be found in prior publications.[23,24]

The NREL clustering analysis was done using the Spectral Clustering method as implemented in scikit-learn.[25] An affinity metric combining both the similarity of XRD patterns and the proximity in composition was used to promote compositionally connected clusters. Specifically

$$A_{ij} = \exp(-\varepsilon(1 - CC_{ij}^{XRD} \cdot (1 - dd_{ij}^{COMP}))^2) \qquad (1)$$

where CC_{ij}^{XRD} is the normalized cross correlation of the xrd patterns and dd_{ij}^{COMP} is the normalized compositional distance. The XRD peak assignment for each of the clusters was performed using reference patterns from the International Centre for Diffraction Data (ICDD) database, also known as powder diffraction file (pdf).

Regardless of the characterization location (NREL or NIST), the libraries synthesized at NREL were measured at 44 points on rectangular 4 × 11 grid covering the 50 × 50 mm substrate. Similarly, the libraries synthesized at NIST were measured at both locations on 177 points on a square 15 × 15 grid truncated to fit a circular 75 mm diameter substrate. In this context, it is important to know that a substantial fraction of time in this comparative study was spent adopting the sample library holders and instrument operation files at NIST and NREL to the new library geometry of the other laboratory. Similarly, it was noted that the data processing tools and interchange protocols for the other laboratory's samples were another bottleneck in the interlaboratory study. Both observations, discussed in more detail below, are important to keep in mind for the future interlaboratory collaborative projects, such as HTE-MC envisioned in literature.[4]

Data was harvested from instruments automatically at NREL and manually at NIST. Data was exchanged internally as tabular data in CSV format, using cloud-based data storage

services, for interlaboratory analysis purposes. The NREL-measured data for both NIST and NREL samples was also made publicly available through NREL's high-throughput experimental materials (HTEM) database at https://htem. nrel.gov/.[26] In addition, to support FAIR (Findable, Accessible, Interoperable, Reusable) data principles,[27] all data in standardized XML format was published at https://hte. registry.nist.gov/ and used for making the final plots reported in this paper. This repository is based on the NIST-developed Materials Data Curation System (MDCS).[28] More details of this data-exchange part of the interlaboratory study will be discussed in a separate paper.

A consequence of each lab using the other's sampling grid is that each lab is measuring properties at nearly the identical composition, barring minor sample library misalignments. This means that the resultant measurements can be compared qualitatively (as in pseudobinary or ternary plots) to identify how well trends in properties are captured, and quantitatively (as in the parity plots) to identify the reproducibility of the actual measurement. To quantitatively assess the similarity or difference between the characterization of the sample libraries at each institution, we compared measurements for several key scalar quantities: film thickness, sheet resistance, band gap (derived from optical spectroscopies), and the position of the first strong diffraction peak (derived from X-ray diffraction measurements). To quantify the similarities and differences, we utilize paired correlation plots and comparative pseudobinary/ ternary plots, along with reporting mean absolute error (MAE) and root mean standard deviation (RMSD).

Differences between property measurements were further assessed for statistical significance using a paired Welch two-sample t test, paired Wilcoxan rank sum test, and Kolmogorov−Smirnov test.[29] These tests assess whether the observed paired differences between measurements are significant or may have occurred due to random chance, and whether the observed data are drawn from the same statistical distribution. We estimate a 95% confidence interval (CI) around the error distribution. Individual property measurements were truncated in this analysis according to their expected measurement error. Film thickness was rounded to the nearest whole number (nm), and band gap was rounded to the nearest 0.1 (eV). All statistical tests were performed using the R environment for statistical computing, version 3.5.2.[30] We also compare results for one vector quantity (X-ray diffractogram) using clustering analysis to determine structurally similar regions in the ternaries, and analyzed the crystallographic identity of each of the resulting clusters.

The differences in the deposition techniques require different presentation methods for the NIST versus the NREL synthesized libraries. The NIST library was deposited as a composition spread with a relatively large composition region covered and is thus presented in the form of pseudoternary plots. The NREL libraries are deposited as heavily doped binary composition spreads and cover substantially less of the ternary and thus are plotted as pseudobinary plots, where the Ti content is considered roughly constant. In both cases, the oxygen content in the film is considered as an implicit variable since it is not directly measured or used in the calculation for the x-axis. No attempt was made in this study to compare the resultant properties of the sputtered and PLD libraries to one another.
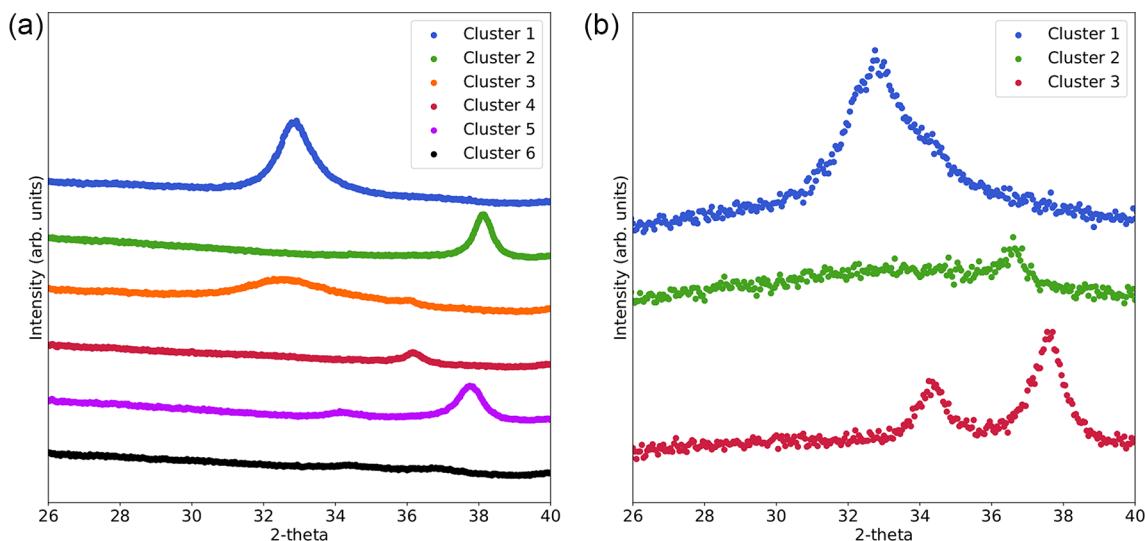
Figure 1. Representative diffraction spectra (a) for each of the 6 clusters identified by the NIST clustering on the NIST sample and (b) for each of the 3 clusters identified by the NREL clustering on the NIST sample.
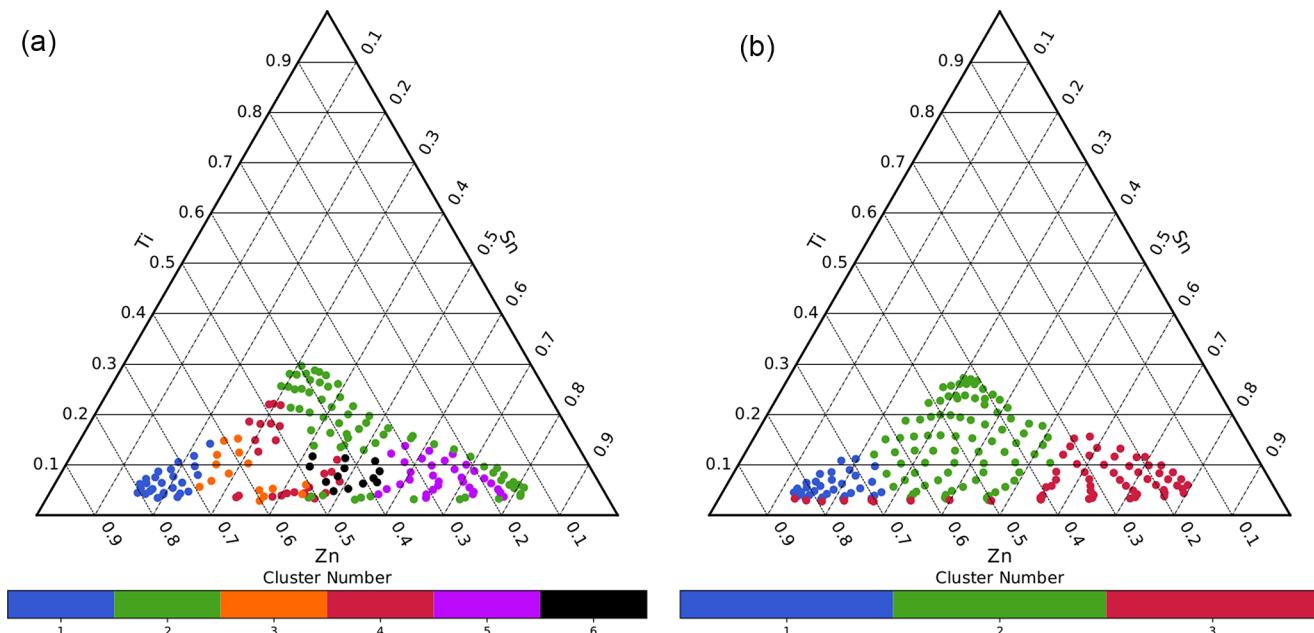

Figure 2. Results from clustering of the X-ray diffractograms gathered and analyzed by (a) NIST and (b) NREL on the NIST-deposited sample graphed as pseudoternary oxides. The cluster number assignments to different phases are discussed in the text.

■ RESULTS AND DISCUSSION

The Zn−Sn−Ti−O library deposited at NIST displayed steep composition spreads, with Zn and Sn varying between 15 cation at.% and 85 cation at.%, and Ti varying between 5 cation at.% and 30 cation at.%. Thus, the resulting plots of properties are shown as ternary diagrams with partially covered composition spread range.

All the diffraction patterns measured at NIST and at NREL are shown in Figure S1 as a function of chemical composition. The trends in the peaks positions are qualitatively similar as a function of Sn content defined as Sn/(Sn + Zn + Ti), with a few small quantitative differences in peak widths and intensities resulting from the use of different collimators and integration times. However, because of the large ternary region covered by the library it is not possible to determine how the phases are distributed in composition space and phase identification is

challenging. For instance, the variation in the Ti concentration in Figure S1 is evidenced by the movement of the peak for nominally identical ratios of Sn/(Sn + Zn + Ti) and complicates analysis from these plots.

To address this problem, clustering analysis of XRD data was performed by each lab, with 6 clusters identified by NIST and 3 clusters identified by NREL. Representative spectra from each cluster were randomly selected for side-by-side comparison and are shown in Figure 1. It appears that NIST clusters 1 and 3 contain the same primary peak as NREL cluster 1, typical for ZnO-type structure (pdf no. 00-065-0725) indicated by a peak close to $2\Theta = 33°$. Furthermore, NIST cluster 4 contains the same peak as NREL cluster 2, which is likely Zn_2SnO_4 structure (pdf no. 04-002-4403) indicated by weak reflections at $2\Theta = 18°$ and $36°$, with some patterns containing an X-ray amorphous material. Finally, NIST clusters
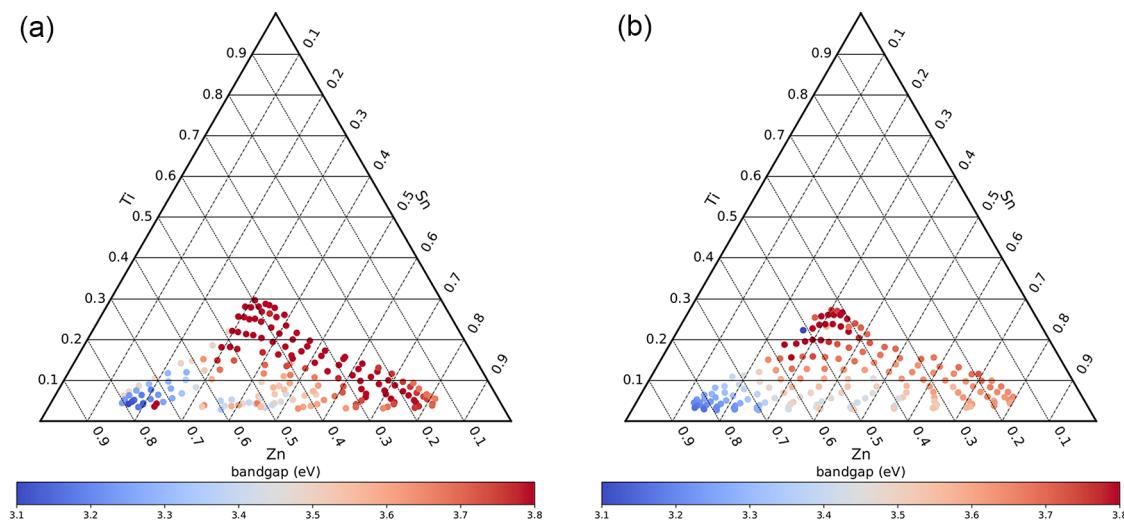
Figure 3. Plots of the pseudoternary oxide Zn−Sn−Ti−O system band gap for the NIST sample as measured by (a) NIST and (b) NREL. Qualitative agreement is observed between the compositional trends despite scatter from electron probe compositional measurements.
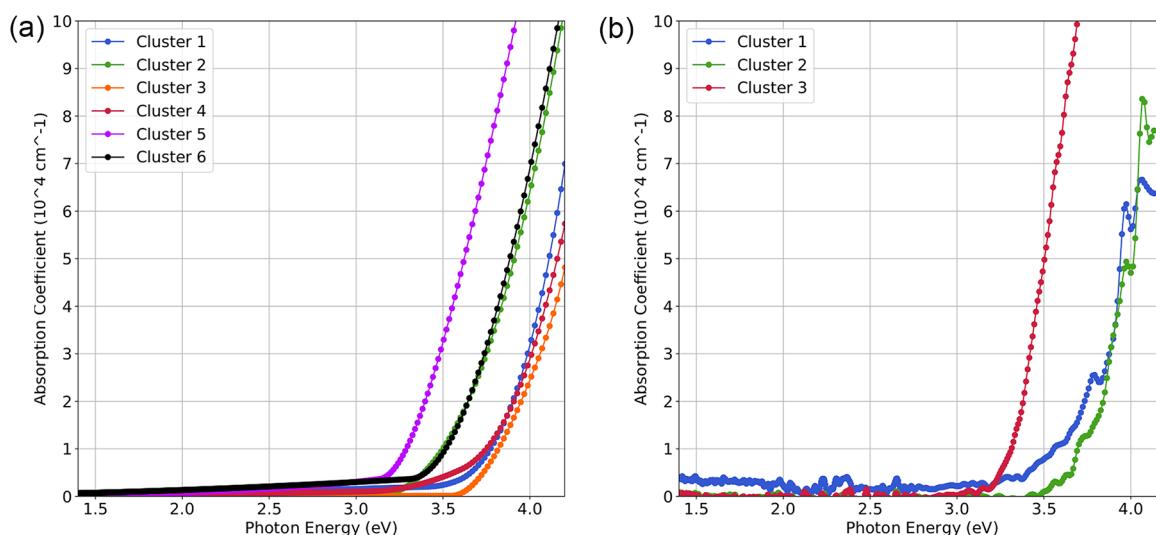

Figure 4. Representative absorption coefficient spectra corresponding to clusters shown in Figure 1 as measured at (a) NIST and (b) NREL.

2 and 5 contain the same primary peak as NREL cluster 3, characteristic of SnO$_2$-like structure (pdf no. 01-075-2893) with a peak at 2Θ = 37° to 38°. Thus, qualitative comparison of the diffraction measurements show the data to be correlated.

Chemical composition regions of 6 clusters identified by the clustering algorithm used at NIST is shown in Figure 2a. Cluster 1 is concentrated in the Zn-rich regions with greater than ∼75 cation at.% Zn. Cluster 2, which resides from the Ti-rich region and down along the Sn−Ti edge of the mapped region. Cluster 3, primarily located at Zn concentrations from 74 cation at.% to 58 cation at.% and is similar to that of cluster 1. Cluster 4 appears to be a distinct phase at lower Zn concentrations compared to that of cluster 3. Cluster 5 appears similar to cluster 2. Finally, cluster 6 is composed of an amorphous phase with no discernible peaks. However, not each of these 6 cluster corresponds to a unique structure, as peak shifting can impact the distance metric used to assign clusters

Using the XRD clustering method implemented at NREL for XRD patterns measured at NREL on NlST sample library leads to a smaller number of clusters (3 total), with

composition regions as shown in Figure 2b. Cluster 1 corresponds to Zn-rich compositions; cluster 3 corresponds to Sn-rich compositions, and cluster #2 corresponds to a phase at intermediate Zn/Sn composition extending further into Ti content. The number of clusters, different from that obtained at NIST, is most likely due to differences in the XRD clustering methods. On the one hand, the NREL method uses composition distance metric to assist with clustering, whereas the NIST method used in this study does not take into account the composition. On the other hand, the NIST method seems to indicate the presence of one-phase and two-phase regions, whereas the NREL method indicates the patterns consist of only single-phase regions.

Although the overall composition region reported in Figure 2a and b is similar, there are clear differences in the measured composition at each point. The compositions provided by NIST were measured via SEM wavelength dispersive spectroscopy (SEM-WDS), which is known to lead to inaccurate elemental analysis for highly insulating samples. Sample libraries were carbon coated prior to SEM-WDS to compensate for their inherent low conductivity, but it appears
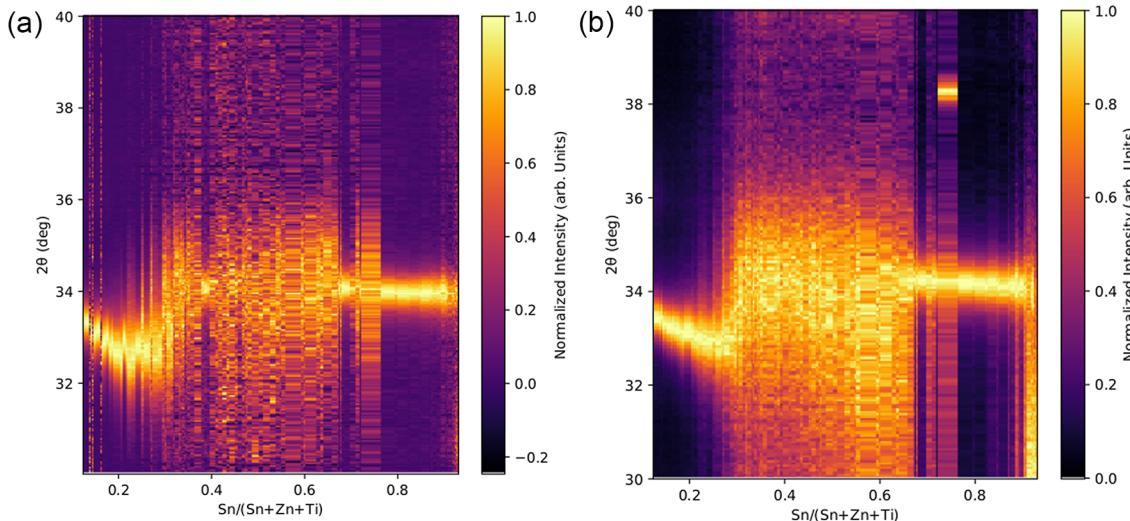
Figure 5. XRD intensity color map as a function of Sn/(Zn + Sn + Ti) composition of the NREL sample as (a) measured by NIST and (b) measured by NREL. The maximum intensity for each XRD pattern is separately normalized to one.

that the coating was either too thin or patchy, leading to large errors in the center of the library. This scatter does not appear to impact qualitative evaluation of the trends in the scalar properties measured and does not impact quantitative comparisons presented later. This is due to the rigorous sample registry used by the participating laboratories, wherein the same position on the library was measured by each laboratory.

The thickness versus composition pseudoternary plots are provided in the Supporting Information (Figures S2 and S3). Briefly, the thickness varied from 60 to 110 nm across the spread, with the maximum thickness in the center of the compositional range. The trend of thickness versus composition for the NREL measurement of the NIST sample libraries is in good qualitative agreement. The center of the ternary is reported to have the highest overall thickness, a maximum value of 96 nm, and the edges of the ternary show values of 47−50 nm.

The sheet resistance for the NIST-synthesized NIST- and NREL-measured Zn−Sn−Ti−O system was difficult to measure because of the high resistivity of the samples synthesized at 500 °C in oxygen environment. Although resistance measurements were attempted at NIST for each of the 177 grid points, actual sheet resistance values could be measured only for the 35 samples, and even then some of these values (10^7−10^8 Ω/sq) were close to the input impedance of the measurement equipment. An additional complicating factor for the measurement is that incorporation of Ti results in a rapid increase in the sheet resistance and hence large changes in resistance over the small measurement area. A similar range of high sheet resistance observed for the NIST measurements is also observed for the NREL measurements. However, the NREL mapping of sheet resistance was able to measure a few additional samples (53 rather than 35), due to manual optimization of the measurement conditions, such as excitation current value, equilibration time, and collection time. Overall, the highly resistive behavior of this library, makes the sheet resistance measurements difficult, and quantitative discrepancies analysis impossible. The interested reader is encouraged to use the Jupyter notebooks contained in the Supporting Information to generate the plots.

Figure 3a plots the bandgap as a function of composition for the NIST synthesized and NIST measured bandgap for the Zn−Sn−Ti−O pseudoternary material system. Overall trends in the variation of bandgap observed are (1) Zn additions decrease the bandgap and (2) Ti additions increase the bandgap. Trend 1 is particularly notable along the Sn−Zn binary edge, where the band gap monotonically decreases as Zn is added to the alloy. The Zn rich region of the phase diagram exhibits the smallest band gap (∼3.1 eV), which is consistent with the value for ZnO of 3.3 eV. The Sn-rich regions exhibit a maximum observed band gap of ∼3.8 eV, which is similar to the reported direct band gap for SnO_2 of 3.6 eV. The addition of Ti similarly increases the band gap, for instance increasing Ti along the 50/50 Sn/Zn line rapidly increases the band gap from 3.4 to 3.8 eV.

The NREL derived band gap values were taken directly from determining the photon energy at which the optical absorption coefficient spectra is at a value of 10^4 cm^{-1} and are displayed in Figure 3b. The overall trends are consistent with those of the NIST values. For instance, the lowest band gaps are observed for the highest Zn concentrations and along the Zn−Sn binary edge there is a monotonic increase in bandgap as Sn content is increased. The NREL data also demonstrate the role of Ti in increasing the band gap, with the largest values for band gap being in the regions containing the most Ti. Figure 4 shows representative absorption coefficient spectra for each cluster (see Figure 1) using the same sample locations as for representative XRD.

For the Zn−Sn−Ti−O libraries deposited by sputtering at NREL, a relatively small Ti composition spread was achieved compared to the sample libraries deposited by PLD at NIST because of the steep angle of the Ti sputtering source with respect to substrate plane. Thus, we choose to display the property measurement data in pseudobinary fashion as a function of Sn cation at.% defined as $x = $ Sn/(Sn + Zn + Ti), where Ti is approximately 5 cation at.% for all samples on the library.

Results of structural characterization of Zn−Sn−Ti−O sample libraries prepared at NREL and measured at NIST and NREL are shown in Figure 5a and b, respectively. The underlying XRD color intensity map is presented in each
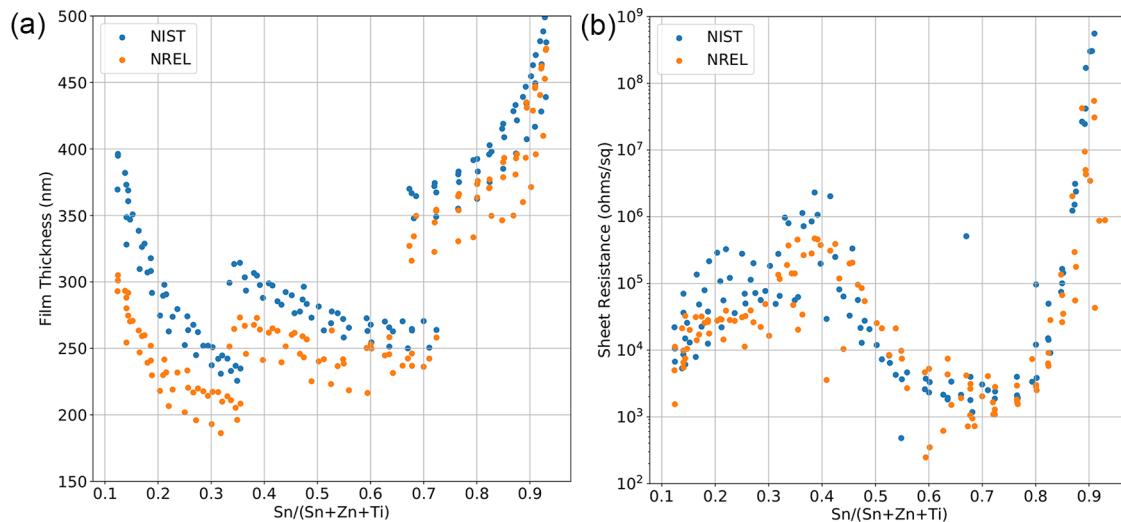
Figure 6. (a) Film thickness and (b) sheet resistance for three NREL Zn−Sn−Ti−O sample libraries, as measured at NREL and NIST. The thickness measured at NREL is underestimated because of an error in XRF measurement of light elements.

figure. The trends in peak position are preserved in both measurements and each measurement can be visually clustered into 3 distinct regions. The Zn-rich samples (Sn cation at.% < 25, cluster 1) show an XRD reflection at $2\Theta = 33.0$ ° to $33.5°$ and other small peaks characteristic of the (002) peak of ZnO-like wurtzite structure (pdf no. 00-065-0725), whereas the Sn-rich samples (Sn cation at.% > 70, cluster 3) show a peak at $2\Theta = 34.2°$ typical of the (101) peak of SnO_2-like rutile structure (pdf no. 01-075-2893). The other peaks of these two structures are missing, likely due to preferential orientation of the films. The films remain XRD-amorphous in the intermediate composition range (40< Sn cation at.% < 60, cluster 2) due to structural frustration and at Sn-rich compositions ($x > 90$ cation at.%) due to sputter source proximity effects. These structural results for the low-Ti Zn−Sn−Ti−O films deposited on heated substrates differ from the previously published combinatorial studies for Ti-free Zn−Sn−O films subjected to postdeposition annealing, where intermediate phases like Zn_2SnO_4 and $ZnSnO_3$ were observed.[31,32] The NIST XRD results for the NREL sample libraries are qualitatively similar, but the peaks tend to have lower width, likely due to smaller size of the X-ray beam.

The thickness measurement results for NREL sample libraries are shown in Figure 6a, as measured at NIST and at NREL as a function of Sn composition, and the pseudoternary plots are shown in Figures S4 and S5. The three distinct groups of thicknesses correspond to the three libraries prepared at NREL to cover the entire Zn/Sn composition spread, as mentioned in the Methods section. The NREL and NIST measurements generally agree regarding the trend of thickness as a function of composition: the samples are thinner in intermediate composition range (200−300 nm), compared to the Zn-rich and Sn-rich edges (up to 400−500 nm). This trend is quite commonly observed in composition spreads prepared by combinatorial sputtering. However, it appears that regardless of the composition, NREL measured thickness is 10−100 nm lower compared to NIST measured thickness, which corresponds to approximately 5% to 25% relative error on per point basis, likely due to measurement of only metallic elements (and not oxygen) in XRF analysis (see more discussion below).

As shown in Figure 6b, the composition trends of sheet resistance measurements at NREL and NIST are in good qualitative agreement. The sheet resistance of the Zn-rich crystalline wurtzite films is $10^4–10^5$ Ohms/sq., which corresponds to 1−10 S/cm. For the Sn-rich crystalline rutile films, the sheet resistance is close to $\sim10^3$ Ohms/sq, corresponding to conductivity of ~10 S/cm. These results are comparable to the previously published literature for similar compositions and comparable deposition conditions.[31] For the amorphous films, the conductivity drops down to 10^{-1} S/cm in intermediate composition range ($0.4 < x < 0.6$) and to 10^{-3} S/cm at very Sn-rich compositions ($x > 0.9$). These low values are likely indicative of low carrier mobility due to high structural disorder in the amorphous films.

The composition dependence of the optical band gap for the sputtered Zn−Sn−Ti−O films deposited at NREL is shown in Figure 7, defined here as the energy at which absorption coefficient is 10^4 cm^{-1}. The full absorption coefficient spectra for the 132 NREL samples are shown in Figure 8 using a
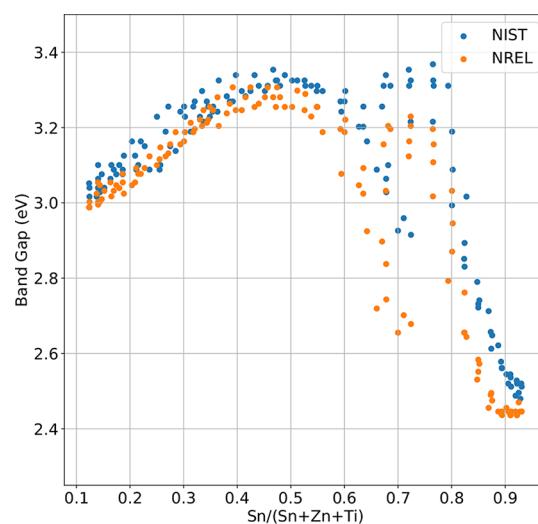

Figure 7. Optical band gap of Zn−Sn−Ti−O thin films deposited at NREL as a function of composition. The compositional trends measured at NREL and NIST are in good agreement with each other.
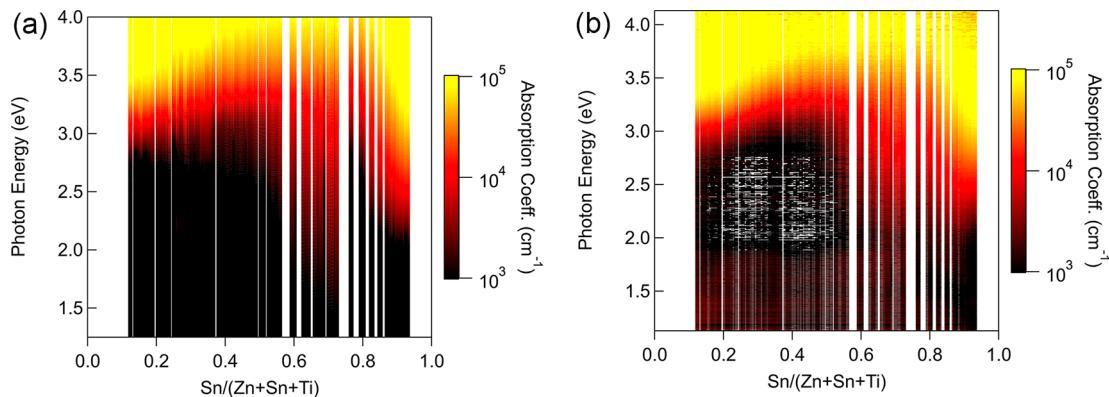
Figure 8. (a) NIST and (b) NREL measured optical absorption coefficient spectra as a function of Sn/(Zn + Sn + Ti) composition for NREL grown samples shown using a logarithmic color scale.

logarithmic color scale. The optical band gap shifts from 3.0 to 3.3 eV with increasing Sn content up to Sn/(Sn + Zn + Ti) = 0.4, where crystalline wurtzite phase is present. At higher Sn content for amorphous films, with exception of the crystalline rutile phase region (onset at 3.3 eV), the absorption onset becomes less sharp and drops down to 2.4 to 2.6 eV for the highest Sn concentrations. Such smearing of the optical absorption with changing chemical composition has been previously observed in SnO-based alloys,[33] and is common for oxides with multiple oxidation states (e.g., Cu_2O-based alloys[34]). Overall, the measured wurtzite and rutile optical absorption onsets are consistent with the GW calculated band gap for ZnO (3.3 eV) and SnO_2 (3.4 eV) available at https://materials.nrel.gov.

Quantitative comparison of the position of the first strong diffraction peak from the measurements performed at NIST and NREL revealed that the two generally agree to within 0.2° 2−θ (Figure 9). The biggest discrepancies between the two measurements occurred when either (1) the first strong diffraction peak had a large full width at half-maximum or (2) the signal-to-noise made differentiating the peak from background in one measurement too difficult. Several attempts were made to automate the peak finding but the presence of

peak shift and multiple phases distorted the parity plots for peak position and full width half-maximum.

Next, we attempt to compare the results from NREL and NIST XRD clustering algorithms (Figure 1 and Figure 2). Overall, NIST and NREL clustering analyses agree on the position of the ZnO and SnO_2 phases, with some disagreement regarding their precise extent. In the case of the NREL data, the additional constraint that compounds with similar compositions must have similar diffraction patterns creates three large clusters that capture the gross trends within the diffraction data (Figure 1b and Figure 2b). The NIST clustering, in contrast, captures additional features, such as the change in SnO_2 texturing, the presence of an amorphous region, and mixed phase regions (Figure 1a and Figure 2b). Neither approach alone is sufficient alone for final phase indexing but either could be used to begin the process of correlating composition, structure and properties.

Figure 10 presents the comparison of NIST and NREL measurements of thickness across all samples. The NIST sample library was roughly 3x thinner than the NREL sample libraries. This is unsurprising since layer-by-layer deposition is slower than codeposition and thus the libraries are typically
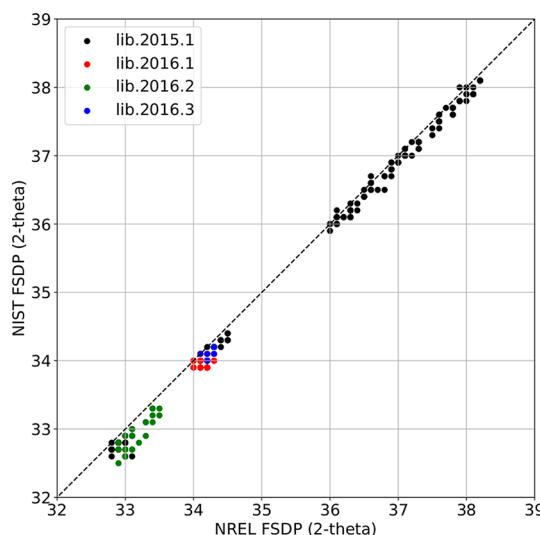

Figure 9. Correlation plot comparing measurements of fwhm of the first strong diffraction peak for NIST (black) and NREL samples (green, blue, and red) measured at each laboratory.
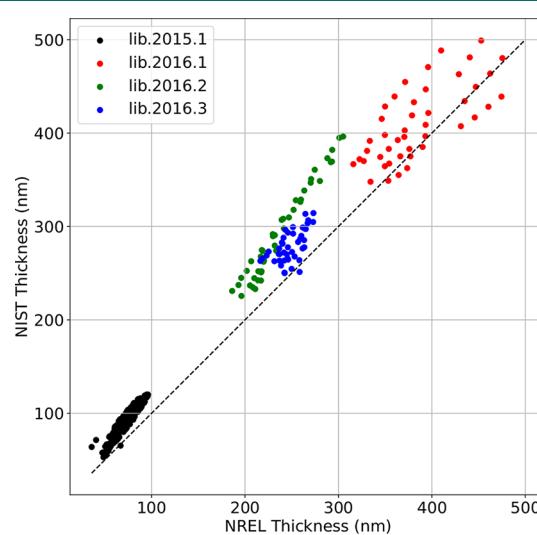

Figure 10. Correlation plot comparing measurements of thickness for NIST (blue) and NREL samples (green, black, and red) measured at each laboratory. The plot shows clearly the tendency of XRF to underestimate the thickness of oxide films.

grown as thin as is practical. In comparison to the NIST values for thickness, the NREL measurements tend to underestimate the film thickness.

The variability in the measured values of thickness from NREL and NIST was relatively large. Over all the measured samples in this study, the mean absolute error (MAE) was 27.5 nm (95% confidence interval 24.2 to 28.8) and the root mean squared deviation (RMSD) was 33.5 nm. These differences are statistically significant for all samples according to the tests used. For only the NIST synthesized samples, the MAE was 18.2 nm and the RMSD was 19.4 nm. These are large values considering the maximum reported thickness of the sample was 120 nm (measured at NIST) and 97 nm (measured at NREL). In the case of the NREL synthesized samples (thickness up to 500 nm), the MAE was 40 nm and the RMSD was 46 nm. The NREL samples are generally thicker than those produced by NIST.

Overall, thickness measurements between NIST and NREL exhibit strong qualitative agreement but only weak quantitative agreement (~10−20% relative error). This relatively large error is likely due to underestimation of the thickness by XRF measurement model in NREL measurement, due to difficulty in measuring oxygen by this technique (not the case for NIST ellipsometry measurements of the thickness). Such error is a well-known shortcoming of using the XRF model to extract the thickness for samples containing light elements. In scientific publications focused on materials properties, this error is commonly corrected at NREL by complementary thickness measurements using profilometry,[35] microscopy,[36] or other techniques. Here, we intentionally did not perform such correction, since the purpose of this study was interlaboratory comparison of the different measurement techniques (rather than correction methods).

Despite the qualitative agreement in the sheet resistance measurements for NREL samples reported above (Figure 6b), there is weaker point-by-point quantitative agreement between the two measurements of these samples measured at NIST and at NREL. Across all samples and measurements, there is an average difference of 0.23 orders of magnitude (95% CI of 0.08 to 0.37). Differences are statistically significant for all but one sample library (2016.3) where the differences are wholly within the expected measurement precision (0.22 mean, CI 0.06 to 0.49) and the measurement results can be considered identical. NIST measurements appear to produce smaller observed resistance relative to NREL. The high resistivity of the samples was the most likely a leading source of disparity in the measurements. Another potential source of error could be the amount of probe force used, which is not information that is automatically captured from the instrument. An additional possible source of error is the different measurement conditions used at different laboratories, such as excitation current, delay time, and collection time, all of which are important to get an accurate measurement for resistive samples.

A comparison of NIST and NREL derived band gaps for all three NREL libraries and the NIST library is presented in Figure 11. The general quantitative agreement between the two sets of measurements is quite good. In comparison to the NREL measurements, the NIST values tend to overestimate the value of the band gap slightly. It is notable that the NIST synthesized samples reported a larger overall bandgap in comparison to the NREL samples. This is likely a result of the synthesis approach, as the NIST samples were deposited in an
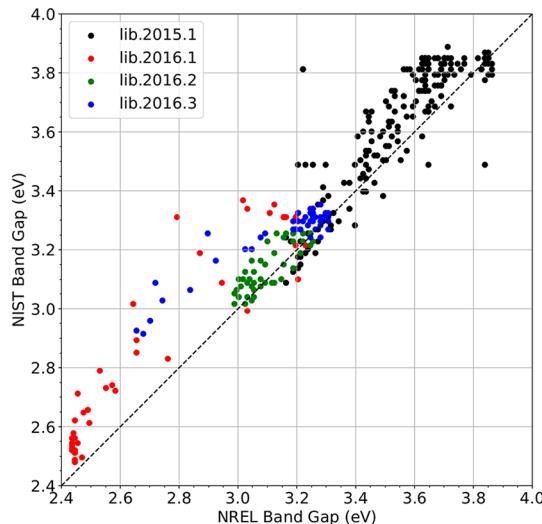

Figure 11. Correlation plot comparing the optical band gaps for NIST (black) and NREL samples (green, blue, and red) measured at each laboratory. The plot shows good correlation between the measurements.

oxygen environment at high temperature and are thus much closer to stoichiometric crystalline oxides, as compared to more disordered materials deposited at lower temperature in Ar environment by NREL to maximize their electrical conductivity.

A simple histogram of the absolute errors for all the samples reveals that 252 of the 309 reported values are within 0.1 eV of one another. The absolute error histogram has a relatively long tail, with 23 of the 309 reported values differing by more than 0.2 eV from one another. The overall mean absolute error (MAE) between the two data sets is 0.10 eV with a root-mean-square error (RMSE) of 0.14 eV and 95% confidence interval between 0.08 and 0.12 eV. Only one of the libraries (2016.2) showed the close agreement with error wholly within the expected measurement precision of 0.1 eV (95% CI = 0.02−0.06 eV). Differences between measurements appear statistically significant for all samples and generally skewed toward smaller measurements at NREL. An aberrantly small band gap in the NREL data for the NIST sample (1.38 eV for sample number 15) was discarded prior to the statistical analysis because of identified measurement procedure error. Considering the two very different methods used, including the shortcomings of the approximations used, the reported band gap values are sufficiently close to allow for both qualitative (e.g., compositional trends) and quantitative comparisons between the laboratories.

This work was conducted between 4 institutions: NIST, NREL, SLAC (additional synchrotron diffraction measurements), and UMD (SEM-WDS measurements). We encountered numerous unexpected issues related to effective communication and data provenance. First, the transfer of library geometry maps was not as straightforward as one might expect, and institutional conventions created ambiguity in merging data from different institutions. For instance, measuring the same point at the beginning and end of a scan but not providing a recording of the x−y coordinates with the data can cause an unexpected +1/−1 shift in position registry. Carefully constructed laboratory notebooks can be (and were) used to untangle these issues, but such notes would not be available on an online data repository and would hinder

data comparison and reproducibility. In terms of minimizing the time spent by technical staff filling out comprehensive meta-data spreadsheets, there is no substitute for having a laboratory information management system (LIMS).[37] Such LIMS systems should be strongly encouraged in the future HTE-MC to reduce difficulties in attempts to compare large volumes of materials property measurements.

Second, even within a single laboratory, following FAIR standards for storing and exchanging data should be encouraged.[27] Over the course of this study, several Excel spreadsheets were generated, (e.g., to correlate optical spectra to composition), but with different formats that also changed slightly as the project proceeded. This led to apparently erroneous values for calculated properties (e.g., bandgap) that were not unphysical but were certainly not representative of the material properties. Once these hurdles were overcome the exchange of scientific information was facile. In particular, the materials data curation system (MDCS) dramatically reduced the amount of time required for data comparison. The code used to create a portion of the figures in this paper is available via the Supporting Information in the form of a Python Jupyter notebook and can be run in less than a minute without the need to lose time reinterpreting Excel worksheets. We encourage the interested reader to run the Jupyter notebooks published with this manuscript to get a feel for how easy it can be to pull data down from the repository and start interacting with it (https://github.com/usnistgov/NIST-NREL-Interlaboratory-Figures). Another great example of this is the HTE X-ray diffraction beamline established at SLAC,[38] where a regularized grid is applied to a few standard wafer sizes and the entire data acquisition and analysis workflow is streamlined to provide users with the data they need when they leave the synchrotron line.

Finally, two additional questions have not been addressed in this study. The question of how best to encode "soft heuristics" (for instance, SEM-WDS is prone to charging on insulating samples and thus compositions can be distorted) will be addressed in a forthcoming manuscript on the data curator. Also, no attempt has been made to compare the data for samples with the same composition that have been prepared under different synthesis conditions or using two different synthesis techniques (e.g., sputtering and PLD in this study). Here, we focused only on comparing the data for the same samples, as measured at two different institutions, which is useful for experimental benchmarking, but insufficient for comparison with theoretical data in various public computational databases.[39−41] To make high-throughput experimental materials data more useful for benchmarking computational data, a similar study addressing comparison between the same deposition techniques at two different institutions, or between different deposition techniques, would be needed in the future. We encourage the interested reader to undertake this study.

CONCLUSIONS

In this Research Article, we report the results of a comparative interlaboratory study of Zn−Sn−Ti−O thin film materials prepared using high-throughput experimental methods. Two sets of Zn−Sn−Ti−O sample libraries were synthesized at NIST and NREL, then measured at each of these two institutions. Sample measurement grids were exchanged between the two laboratories to ensure measurements were made at the same points (e.g., compositions) and the data and meta-data were exchanged using the materials data curation

system. The optical band gaps determined at NIST and NREL on the same samples are in good quantitative agreement with each other (0.1−0.2 eV error), despite two different measurement techniques (ellipsometry vs spectroscopy). The thickness measurements performed using XRF are systematically underestimated compared to thicknesses extracted from the ellipsometry models (25−30 nm error), likely due to inability of XRF to detect light elements like oxygen. The sheet resistance determined using 4-point probe vary by 0.08−0.37 orders of magnitude, due to a combination of measurement difficulty (high sample resistance) and different measurement geometries (radial vs rectangular probe orientation). These technical results, as well as additional lessons learned as a part of this study, stress the importance of developing and executing rigorous protocols for sample library measurement and data exchange in future interlaboratory and round-robin studies. Overall, this Research Article serves as a proof of concept for exchanging samples and data within the future High-Throughput Experimental Materials Collaboratory (HTE-MC).

■ ASSOCIATED CONTENT

ⓢ Supporting Information

The Supporting Information is available free of charge on the ACS Publications website at DOI: 10.1021/acscombsci.8b00158.

> Details of the ellipsometric modeling performed at NIST (PDF)

> All the code and files necessary to download all data taken during this study from the HTE Materials Registry, as well as the code used to generate all figures except Figure 8a and b (ZIP)

■ AUTHOR INFORMATION

Corresponding Author

*E-mail: martin.green@nist.gov. Tel: 301-975-8496.

ORCID ⓘ

Jason R. Hattrick-Simpers: 0000-0003-2937-3188
Andriy Zakutayev: 0000-0002-3054-5525
Apurva Mehta: 0000-0003-0870-6932
Ichiro Takeuchi: 0000-0003-2625-0553

Notes

Certain commercial equipment, instruments, or materials are identified in this Research Article to foster understanding. Such identification does not imply recommendation or endorsement by the National Institute of Standards and Technology nor does it imply that the products or services identified are necessarily the best available for the purpose.

The authors declare no competing financial interest.

■ ACKNOWLEDGMENTS

■ REFERENCES

(1) Xiao-Dong, X.; Takeuchi, I. *Combinatorial Materials Synthesis*; CRC Press, 2003.

(2) Potyrailo, R.; Amis, E. J. *High-Throughput Analysis: A Tool for Combinatorial Materials Science*; Springer Science & Business Media, 2012.

(3) Green, M. L.; Takeuchi, I.; Hattrick-Simpers, J. R. Applications of High Throughput (Combinatorial) Methodologies to Electronic, Magnetic, Optical, and Energy-Related Materials. *J. Appl. Phys.* **2013**, *113* (23), 231101.

(4) Green, M. L.; Choi, C. L.; Hattrick-Simpers, J. R.; Joshi, A. M.; Takeuchi, I.; Barron, S. C.; Campo, E.; Chiang, T.; Empedocles, S.; Gregoire, J. M.; et al. Fulfilling the Promise of the Materials Genome Initiative with High-Throughput Experimental Methodologies. *Appl. Phys. Rev.* **2017**, *4* (1), 011105.

(5) Rajan, K. Combinatorial Materials Sciences: Experimental Strategies for Accelerated Knowledge Discovery. *Annu. Rev. Mater. Res.* **2008**, *38* (1), 299−322.

(6) Maier, W. F. F.; Stöwe, K.; Sieg, S. Combinatorial and High-Throughput Materials Science. *Angew. Chem., Int. Ed.* **2007**, *46* (32), 6016−6067.

(7) Otani, M.; Lowhorn, N. D.; Schenck, P. K.; Wong-Ng, W.; Green, M. L.; Itaka, K.; Koinuma, H. A High-Throughput Thermoelectric Power-Factor Screening Tool for Rapid Construction of Thermoelectric Property Diagrams. *Appl. Phys. Lett.* **2007**, *91* (13), 132102.

(8) Barron, S. C.; Gorham, J. M.; Patel, M. P.; Green, M. L. High-Throughput Measurements of Thermochromic Behavior in V $_{1−X}$ Nb $_X$ O $_2$ Combinatorial Thin Film Libraries. *ACS Comb. Sci.* **2014**, *16* (10), 526−534.

(9) Cui, J.; Chu, Y. S.; Famodu, O. O.; Furuya, Y.; Hattrick-Simpers, J.; James, R. D.; Ludwig, A.; Thienhaus, S.; Wuttig, M.; Zhang, Z. Y. Combinatorial Search of Thermoelastic Shape-Memory Alloys with Extremely Small Hysteresis Width. *Nat. Mater.* **2006**, *5* (4), 286−290.

(10) Löbel, R.; Thienhaus, S.; Savan, A.; Ludwig, A. Combinatorial Fabrication and High-Throughput Characterization of a Ti−Ni−Cu Shape Memory Thin Film Composition Spread. *Mater. Sci. Eng., A* **2008**, *481−482*, 151−155.

(11) Otani, M.; Lowhorn, N. D.; Schenck, P. K.; Wong-Ng, W.; Green, M. L.; Itaka, K.; Koinuma, H. A High-Throughput Thermoelectric Power-Factor Screening Tool for Rapid Construction of Thermoelectric Property Diagrams. *Appl. Phys. Lett.* **2007**, *91* (13), 132102.

(12) de Souza Lucas, F. W.; Zakutayev, A. Research Update: Emerging Chalcostibite Absorbers for Thin-Film Solar Cells. *APL Mater.* **2018**, *6* (8), 084501.

(13) Baranowski, L. L.; Zawadzki, P.; Lany, S.; Toberer, E. S.; Zakutayev, A. A Review of Defects and Disorder in Multinary Tetrahedrally Bonded Semiconductors. *Semicond. Sci. Technol.* **2016**, *31* (12), 123004.

(14) Elmer, K.; Klein, A.; Rech, B. *Transparent Conductive Zinc Oxide*; Springer, 2008.

(15) Wagner, J. F.; Keszler, D. A.; Presley, R. E. *Transparent Electronics*; Springer: US, 2008.

(16) Iwasaki, T.; Itagaki, N.; Den, T.; Kumomi, H.; Nomura, K.; Kamiya, T.; Hosono, H. Combinatorial Approach to Thin-Film Transistors Using Multicomponent Semiconductor Channels: An Application to Amorphous Oxide Semiconductors in In−Ga−Zn−O System. *Appl. Phys. Lett.* **2007**, *90* (24), 242114.

(17) Kim, B. K.; Park, J. S.; Kim, D. H.; Chung, K. B. Semiconducting Properties of Amorphous GaZnSnO Thin Film Based on Combinatorial Electronic Structures. *Appl. Phys. Lett.* **2014**, *104* (18), 182106.

(18) Bassim, N. D.; Schenck, P. K.; Otani, M.; Oguchi, H. Model, Prediction, and Experimental Verification of Composition and Thickness in Continuous Spread Thin Film Combinatorial Libraries Grown by Pulsed Laser Deposition. *Rev. Sci. Instrum.* **2007**, *78* (7), 072203.

(19) Long, C. J.; Hattrick-Simpers, J.; Murakami, M.; Srivastava, R. C.; Takeuchi, I.; Karen, V. L.; Li, X. Rapid Structural Mapping of Ternary Metallic Alloy Systems Using the Combinatorial Approach and Cluster Analysis. *Rev. Sci. Instrum.* **2007**, *78* (7), 072217.

(20) Ndione, P. F.; Zakutayev, A.; Kumar, M.; Packard, C. E.; Berry, J. J.; Perkins, J. D.; Ginley, D. S. Tuning the Physical Properties of Amorphous In−Zn−Sn−O Thin Films Using Combinatorial Sputtering. *MRS Commun.* **2016**, *6* (4), 360−366.

(21) Fioretti, A. N.; Zakutayev, A.; Moutinho, H.; Melamed, C.; Perkins, J. D.; Norman, A. G.; Al-Jassim, M.; Toberer, E. S.; Tamboli, A. C. Combinatorial Insights into Doping Control and Transport Properties of Zinc Tin Nitride. *J. Mater. Chem. C* **2015**, *3* (42), 11017−11028.

(22) He, F.; Van Espen, P. J. General Approach for Quantitative Energy Dispersive X-Ray Fluorescence Analysis Based on Fundamental Parameters. *Anal. Chem.* **1991**, *63*, 2237.

(23) Zakutayev, A.; Perkins, J. D.; Parilla, P. A.; Widjonarko, N. E.; Sigdel, A. K.; Berry, J. J.; Ginley, D. S. Zn−Ni−Co−O Wide-Band-Gap P-Type Conductive Oxides with High Work Functions. *MRS Commun.* **2011**, *1* (1), 23−26.

(24) Fioretti, A. N.; Schwartz, C. P.; Vinson, J.; Nordlund, D.; Prendergast, D.; Tamboli, A. C.; Caskey, C. M.; Tuomisto, F.; Linez, F.; Christensen, S. T.; et al. Understanding and Control of Bipolar Self-Doping in Copper Nitride. *J. Appl. Phys.* **2016**, *119* (18), 181508.

(25) Pedregosa, F.; Varoquaux, G.; Gramfort, A.; Michel, V.; Thirion, B.; Grisel, O.; Blondel, M.; Prettenhofer, P.; Weiss, R.; Dubourg, V.; et al. Scikit-Learn: Machine Learning in Python. *J. Mach. Learn. Res.* **2011**, *12* (Oct), 2825−2830.

(26) Zakutayev, A.; Wunder, N.; Schwarting, M.; Perkins, J. D.; White, R.; Munch, K.; Tumas, W.; Phillips, C. An Open Experimental Database for Exploring Inorganic Materials. *Sci. Data* **2018**, *5*, 180053.

(27) Wilkinson, M. D.; Dumontier, M.; Aalbersberg, Ij. J.; Appleton, G.; Axton, M.; Baak, A.; Blomberg, N.; Boiten, J.-W.; da Silva Santos, L. B.; Bourne, P. E.; et al. The FAIR Guiding Principles for Scientific Data Management and Stewardship. *Sci. Data* **2016**, *3*, 160018.

(28) Dima, A.; Bhaskarla, S.; Becker, C.; Brady, M.; Campbell, C.; Dessauw, P.; Hanisch, R.; Kattner, U.; Kroenlein, K.; Newrock, M.; et al. Informatics Infrastructure for the Materials Genome Initiative. *JOM* **2016**, *68* (8), 2053−2064.

(29) Triola, M. F.; Iossi, L. *Elementary Statistics*; Pearson, 2017.

(30) *R: A Language and Environment for Statistical Computing*; R Foundation for Statistical Computing. R Core Team, 2018.

(31) Ko, J. H.; Kim, I. H.; Kim, D.; Lee, K. S.; Lee, T. S.; Cheong, B.; Kim, W. M. Transparent and Conducting Zn-Sn-O Thin Films Prepared by Combinatorial Approach. *Appl. Surf. Sci.* **2007**, *253* (18), 7398−7403.

(32) Perkins, J. D.; del Cueto, J. A.; Alleman, J. L.; Warmsingh, C.; Keyes, B. M.; Gedvilas, L. M.; Parilla, P. A.; To, B.; Readey, D. W.; Ginley, D. S. Combinatorial Studies of Zn-Al-O and Zn-Sn-O Transparent Conducting Oxide Thin Films. *Thin Solid Films* **2002**, *411* (1), 152−160.

(33) Bikowski, A.; Holder, A.; Peng, H.; Siol, S.; Norman, A.; Lany, S.; Zakutayev, A. Synthesis and Characterization of (Sn,Zn)O Alloys. *Chem. Mater.* **2016**, *28* (21), 7765−7772.

(34) Zakutayev, A.; Stevanovic, V.; Lany, S. Non-Equilibrium Alloying Controls Optoelectronic Properties in Cu_2O Thin Films for Photovoltaic Absorber Applications. *Appl. Phys. Lett.* **2015**, *106* (12), 123903.

(35) Siol, S.; Dhakal, T. P.; Gudavalli, G. S.; Rajbhandari, P. P.; DeHart, C.; Baranowski, L. L.; Zakutayev, A. Combinatorial Reactive Sputtering of In_2S_3 as an Alternative Contact Layer for Thin Film Solar Cells. *ACS Appl. Mater. Interfaces* **2016**, *8* (22), 14004−14011.

(36) Mokurala, K.; Baranowski, L. L.; de Souza Lucas, F. W.; Siol, S.; van Hest, M. F. A. M.; Mallick, S.; Bhargava, P.; Zakutayev, A. Combinatorial Chemical Bath Deposition of CdS Contacts for Chalcogenide Photovoltaics. *ACS Comb. Sci.* **2016**, *18* (9), 583−589.

(37) White, R. R.; Munch, K. Handling Large and Complex Data in a Photovoltaic Research Institution Using a Custom Laboratory

Information Management System. *MRS Online Proc. Libr.* **2014**, DOI: 10.1557/opl.2014.31.

(38) Gregoire, J. M.; Van Campen, D. G.; Miller, C. E.; Jones, R. J. R.; Suram, S. K.; Mehta, A. High-Throughput Synchrotron X-Ray Diffraction for Combinatorial Phase Mapping. *J. Synchrotron Radiat.* **2014**, *21*, 1262−1268.

(39) Curtarolo, S.; Setyawan, W.; Wang, S. D.; Xue, J. K.; Yang, K. S.; Taylor, R. H.; Nelson, L. J.; Hart, G. L. W.; Sanvito, S.; Buongiorno-Nardelli, M.; et al. AFLOWLIB.ORG: A Distributed Materials Properties Repository from High-Throughput Ab Initio Calculations. *Comput. Mater. Sci.* **2012**, *58*, 227−235.

(40) Choudhary, K.; Kalish, I.; Beams, R.; Tavazza, F. High-Throughput Identification and Characterization of Two-Dimensional Materials Using Density Functional Theory. *Sci. Rep.* **2017**, *7* (1), 5179.

(41) Kirklin, S.; Saal, J. E.; Meredig, B.; Thompson, A.; Doak, J. W.; Aykol, M.; Rühl, S.; Wolverton, C. The Open Quantum Materials Database (OQMD): Assessing the Accuracy of DFT Formation Energies. *npj Comput. Mater.* **2015**, *1* (1), 15010.